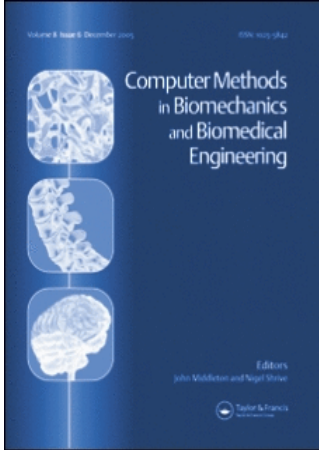


This article was downloaded by:[Imperial College]  
On: 5 January 2008  
Access Details: [subscription number 772812366]  
Publisher: Taylor & Francis  
Informa Ltd Registered in England and Wales Registered Number: 1072954  
Registered office: Mortimer House, 37-41 Mortimer Street, London W1T 3JH, UK



## Computer Methods in Biomechanics and Biomedical Engineering

Publication details, including instructions for authors and subscription information:  
<http://www.informaworld.com/smpp/title~content=t713455284>

### Can the modified Allen's test always detect sufficient collateral flow in the hand? A computational study

J. Alastruey<sup>ab</sup>, K. H. Parker<sup>b</sup>, J. Peiró<sup>a</sup>, S. J. Sherwin<sup>a</sup>

<sup>a</sup> Department of Aeronautics, Imperial College London, London, UK

<sup>b</sup> Department of Bioengineering, Imperial College London, London, UK

Online Publication Date: 01 December 2006

To cite this Article: Alastruey, J., Parker, K. H., Peiró, J. and Sherwin, S. J. (2006) 'Can the modified Allen's test always detect sufficient collateral flow in the hand? A computational study', *Computer Methods in Biomechanics and Biomedical Engineering*, 9:6, 353 - 361

To link to this article: DOI: 10.1080/10255840600985477

URL: <http://dx.doi.org/10.1080/10255840600985477>

PLEASE SCROLL DOWN FOR ARTICLE

Full terms and conditions of use: <http://www.informaworld.com/terms-and-conditions-of-access.pdf>

This article maybe used for research, teaching and private study purposes. Any substantial or systematic reproduction, re-distribution, re-selling, loan or sub-licensing, systematic supply or distribution in any form to anyone is expressly forbidden.

The publisher does not give any warranty express or implied or make any representation that the contents will be complete or accurate or up to date. The accuracy of any instructions, formulae and drug doses should be independently verified with primary sources. The publisher shall not be liable for any loss, actions, claims, proceedings, demand or costs or damages whatsoever or howsoever caused arising directly or indirectly in connection with or arising out of the use of this material.

# Can the modified Allen's test always detect sufficient collateral flow in the hand? A computational study

J. ALASTRUEY<sup>†‡</sup>, K. H. PARKER<sup>‡</sup>, J. PEIRÓ<sup>†</sup> and S. J. SHERWIN<sup>†\*</sup>

<sup>†</sup>Department of Aeronautics, Imperial College London, South Kensington Campus, London SW7 2AZ, UK  
<sup>‡</sup>Department of Bioengineering, Imperial College London, South Kensington Campus, London SW7 2AZ, UK

(Received 10 January 2006; in final form 15 August 2006)

Blood flow in the largest arteries of the arm up to the digital arteries is numerically modelled using the one-dimensional equations of pressure and flow wave propagation in compliant vessels. The model can be applied to different anatomies of arterial networks and can simulate compression of arteries, these allowing us to simulate the modified Allen's test (MAT) and to assess its suitability for the detection of sufficient collateral flow in the hand if radial blood supply is interrupted. The test measures blood flow in the superficial palmar arch before and during compression of the radial artery. The absence of reversal flow in the palmar arch with the compression indicates insufficient collateral flow and is referred to as a positive MAT. This study shows that small calibres of the superficial palmar arch and insufficient compression of the radial artery can lead to false-positive results. Measurement of the drop in digital systolic pressures with compression of the radial artery has proved to be a more sensitive test to predict the presence of sufficient ulnar collateral flow in networks with small calibres of the superficial palmar arch. However, this study also shows that digital pressure measurements can fail in detecting enough collateral flow if the radial artery is insufficiently compressed.

**Keywords:** Modified Allen's test; Hand haemodynamics; Collateral flow; One-dimensional model

## 1. Introduction

The hand is perfused by the ulnar artery (UA) and the radial artery (RA), both of which branch off of the brachial artery (BA) usually below the elbow (figure 1, left). The UA and the RA anastomose across the hand in the form of a superficial palmar arch (SPA) and a deep palmar arch (DPA) that provide collateral flow pathways to the digital arteries, the SPA being the most important route. However, arterial anatomical variations are frequent, with an incomplete SPA reported in approximately 30–40% of subjects (Lippert and Pabst 1985, Olave *et al.* 1993, Moraes *et al.* 2003).

It is of clinical interest to determine the presence of sufficient ulnar collateral flow through the SPA or the DPA to assess whether the RA can be harvested to be used as a coronary artery bypass graft without ischemic complications (insufficient blood supply) to the hand, particularly the thumb and index finger (Kamienski and Barnes 1976, Pola *et al.* 1996, Serricchio *et al.* 1999, Starnes *et al.* 1999, Winterer *et al.* 2001, Zimmerman *et al.* 2001, Broadman *et al.* 2002, Zhen *et al.* 2002). Furthermore, the RA is also

a favourable access for haemodialysis if ulnar collateral flow is present (Kapoian *et al.* 1999). The modified Allen's test (MAT) is a common technique to detect the presence of sufficient ulnar collateral flow. It consists of measuring blood flow in the radial part of the SPA (SPA III) by Doppler ultrasonography (US) before and during compression of the RA at the wrist. The presence of reversal flow (towards the RA) is considered to be an indicator of adequate collateral flow across the palm, and is identified as a negative MAT.

Several authors have studied the reliability of the MAT. Studies by Pola *et al.* (1996), Serricchio *et al.* (1999) and Zimmerman *et al.* (2001) showed that all the follow-up patients who underwent harvesting of the RA after a negative MAT did not present signs of hand ischemia. However, a study with 129 patients by Starnes *et al.* (1999) showed that the test may unnecessarily exclude some patients for RA graft or RA access for haemodialysis (false-positive) and may also place a number of patients at risk of hand ischemia (false-negative). Kamienski and Barnes (1976) reported a 73% false-positive rate of the MAT.

\*Corresponding author. Email: s.sherwin@imperial.ac.uk

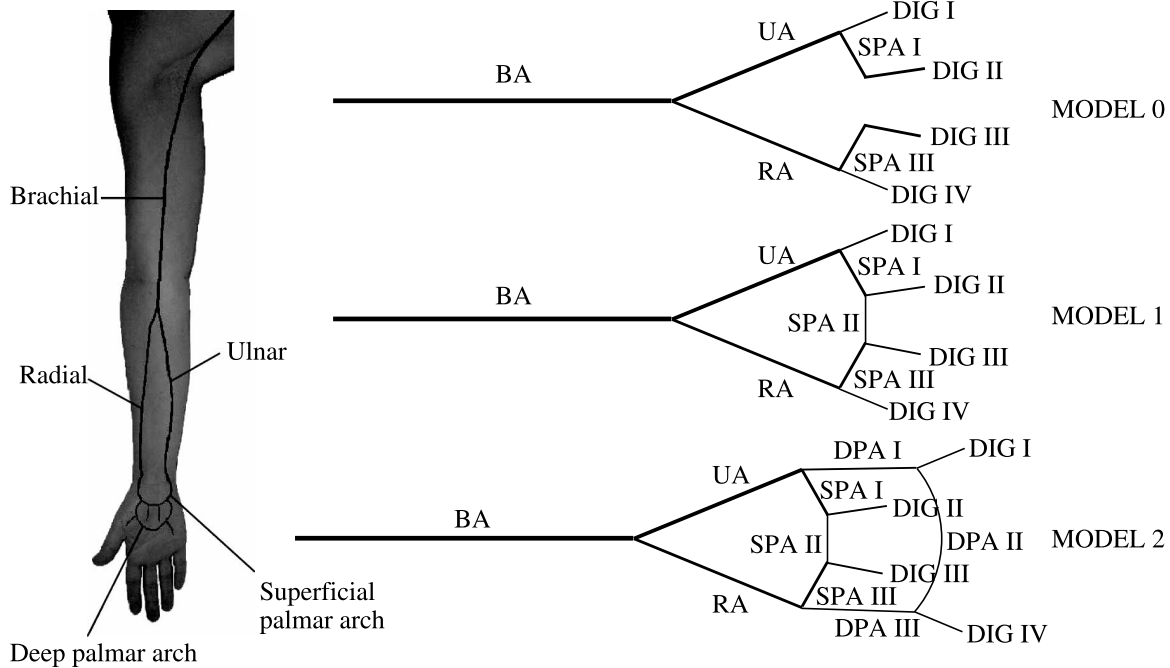


Figure 1. Anatomy of the largest arteries in the arm (left). Schematic of the three anatomically different models studied (right). They contain the brachial artery (BA), the ulnar artery (UA), the radial artery (RA), the superficial palmar arch (SPA I, SPA II and SPA III), the deep palmar arch (DPA I, DPA II and DPA III), and the digital arteries (DIG I, DIG II, DIG III and DIG IV). The thumb is perfused by DIG IV.

In this work, we apply a previously published (Sherwin *et al.* 2003) non-linear, one-dimensional (1-D) model of pressure and flow pulse wave propagation in compliant vessels to simulate the MAT in the three most prevalent arterial anatomies formed by the largest arteries in the arm (figure 1, right). We have a network without either a complete SPA or DPA that we call *Model 0*, a network with a complete SPA that we call *Model 1* and a network with both a complete SPA and DPA that we call *Model 2*. We focus our study on analysing if small calibres of the middle SPA (SPA II) and insufficient compression of the RA are responsible for false-positive or false-negative results of the MAT. When a false result occurs, we analyse if the alternative technique used by Starnes *et al.* (1999) can assess the presence of sufficient ulnar collateral flow better. This technique consists of measuring the change in the systolic pressure of the digital arteries III and IV with the compression of the RA. Pressures are measured with a digital pressure cuff placed on the proximal phalanx. A decrease in digital systolic pressure of 40 mmHg or less is considered to be an indicator of sufficient collateral flow.

## 2. Methodology

### 2.1 Mathematical model

**2.1.1 Governing equations.** The mathematical model is based on the non-linear, 1-D equations of pressure and flow wave propagation in compliant vessels. The governing system of equations results from conservation of mass and momentum applied to a 1-D impermeable and

deformable tubular control volume of incompressible and Newtonian fluid. It takes the form (Sherwin *et al.* 2003, Alastruey 2006):

$$\frac{\partial A}{\partial t} + \frac{\partial(AU)}{\partial x} = 0, \quad (1)$$

$$\frac{\partial U}{\partial t} + U \frac{\partial U}{\partial x} = -\frac{1}{\rho} \frac{\partial p}{\partial x} + \frac{f}{\rho A}, \quad (2)$$

where  $x$  is the axial coordinate along the vessel,  $t$  is the time,  $A(x, t)$  is the cross-sectional area of the vessel,  $U(x, t)$  is the average axial velocity,  $p(x, t)$  is the average internal pressure over the cross-section,  $\rho$  is the density of the blood taken here to be  $1050 \text{ kg m}^{-3}$ , and  $f(x, t)$  is the friction force per unit length, which is modelled as  $f = -22\pi\mu U$  according to Smith *et al.* (2001), with  $\mu$  the viscosity of the blood taken here to be  $4.5 \text{ mPa s}$ .

The system of equations is completed with a pressure-area relation previously used in Olufsen (1999), Sherwin *et al.* (2003) and Alastruey (2006). It assumes a thin, homogeneous and elastic arterial wall and it takes the form:

$$p = p_0 + \frac{\beta}{A_0} (\sqrt{A} - \sqrt{A_0}), \quad \beta = \frac{\sqrt{\pi} h E}{(1 - \sigma^2)}, \quad (3)$$

where  $A_0$  and  $h$  are the sectional area and wall thickness at the reference state ( $p_0, U_0$ ) (with  $p_0$  and  $U_0$  assumed to be zero),  $E$  is the Young's modulus, and  $\sigma$  is the Poisson's ratio, typically taken to be  $\sigma = 1/2$  since biological tissue is practically incompressible. The parameter  $\beta$  is related to

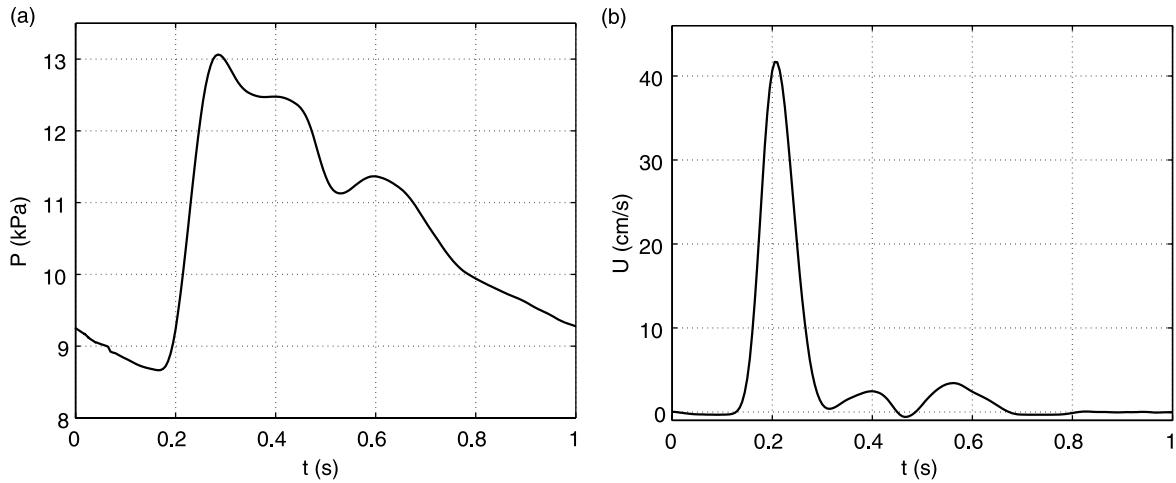


Figure 2. *In vivo* pressure (left), measured with planar tonometry, and velocity (right), measured with Doppler US, over one cardiac cycle at the proximal part of the left subclavian artery.

the speed of pulse wave propagation,  $c$ , through (Sherwin *et al.* 2003, Alastruey 2006):

$$c^2 = \frac{\beta}{2\rho A_0} A^{1/2}. \quad (4)$$

**2.1.2 Treatment of boundary conditions and bifurcations.** The hyperbolic system of partial differential equations (1)–(3) is solved in each arterial segment of the networks shown in figure 1 (right) with the following boundary conditions. At the proximal end of the BA we prescribe the flow time history shown in figure 2 (right), measured with Doppler US at the left subclavian artery of a healthy young adult. Boundary conditions of the arterial segments joining at junctions are prescribed by enforcing conservation of mass and continuity of the total pressure  $p + (1/2)\rho U^2$ . The distal end of each digital artery is coupled to a three-element lumped parameter model (figure 3), consisting of two resistances,  $R_1$  and  $R_2$ , and a compliance,  $C$ , to account for both the resistive and the compliant effects of vessels and microcirculation beyond the distal boundary. It is governed by the differential equation

$$p_{1D} + R_2 C \frac{dp_{1D}}{dt} = p_v + (R_1 + R_2) Q_{1D} + R_1 R_2 C \frac{dQ_{1D}}{dt}, \quad (5)$$

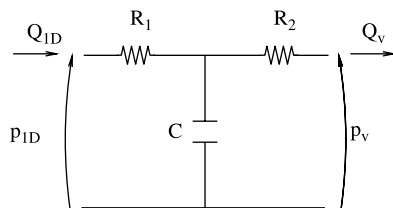


Figure 3. Electrical circuit analogous to the three-element lumped parameter model that simulates the resistance and compliance of vessels and microcirculation beyond the 1-D digital arteries.

where  $p_{1D}$  and  $Q_{1D}$  are the pressure and volume flow rate at the distal end of the 1-D digital artery, and  $p_v$  represents the pressure at the entrance of the venous system, taken to be zero.

At any point in the network we can simulate a compression leading to total occlusion by enforcing the condition  $U = 0$  at the compression point, and a compression leading to partial occlusion by decreasing the calibre of the artery locally (Section 3.3).

**2.1.3 Numerical scheme.** Equations (1) and (2) are solved for area and velocity after substitution of equation (3) into equation (2) to express the term  $\partial p / \partial x$  as  $\partial A / \partial x$  (Sherwin *et al.* 2003, Alastruey 2006). A discontinuous Galerkin scheme with a spectral/ $hp$  spatial discretisation and a second-order Adams–Bashforth time-integration scheme is used. Details on this algorithm can be found in Sherwin *et al.* (2003) and Karniadakis and Sherwin (2003).

Equation (5) is solved using a first-order time discretisation, taking into account that  $p_{1D}$  and  $Q_{1D}$  can be related to  $A_{1D}$  and  $U_{1D}$  (their corresponding  $A$  and  $U$  values at the outlet of each 1-D digital artery) through equation (3) and  $Q_{1D} = A_{1D} U_{1D}$ . This lumped parameter model is coupled to the 1-D digital arteries by solving a Riemann problem at their interface.

The accuracy of our 1-D formulation and the three-element lumped parameter model has been successfully validated in Alastruey (2006).

**2.2 Physiological data**

The physiological parameters used in each arterial network are given in the tables of Appendix A. They are referred to as the control case data. We aim at representing the arterial geometry and elasticity of healthy young adult arms. In the absence of detailed knowledge of these properties, the lengths,  $l$ , and initial radii,  $R_0$ , of the BA, UA and RA are based on data published in Stergiopoulos

*et al.* (1992). The remaining lengths are estimated from an anatomical atlas (Martini 1995), whereas the remaining  $R_0$ 's are assumed to have an area ratio at bifurcations (ratio of the total cross-sectional area of the daughter vessels to that of the parent vessels) close to 1.2. This value yields minimal wave reflection at a bifurcation for forward travelling waves (Gosling *et al.* 1971, Greenwald and Newman 1982, Papageorgiou and Jones 1987). The wall thickness of each artery,  $h$ , is assumed to be 10% of  $R_0$ . We determine  $E$  in each vessel by enforcing the relation  $(A_{01}/c_{01}) = (A_{02}/c_{02}) + (A_{03}/c_{03})$  at each junction, where  $A_{01}$  and  $c_{01}$  are, respectively, the initial area and wave speed of the parent artery, and  $A_{02}$ ,  $c_{02}$ ,  $A_{03}$  and  $c_{03}$  are the corresponding parameters in the two daughter vessels. This is equivalent, under the assumption of small perturbations, to a well-matched bifurcation for forward travelling waves (Sherwin *et al.* 2003, Alastruey 2006).

At the distal end of each digital artery, we assume  $R_1$  to be equal to the characteristic impedance of the terminal branch,  $Z_0 = (\rho c_0/A_0)$  with  $c_0 = c(A_0)$  (4), since it is the value that minimizes the total impedance of the RCR lumped parameter model (Rainest *et al.* 1974). Each peripheral resistance  $R_p = R_1 + R_2$  is obtained by distributing the resistance of the entire network,  $R_N$ , so that the mean outflow rates over one cardiac cycle in the digital arteries are proportional to the corresponding initial cross-sectional areas. The value of  $R_N$  is calculated as the ratio between the mean pressure shown in figure 2 (left) and the mean flow rate measured *in vivo* at the proximal part of the left subclavian artery. The mean flow rate is determined by multiplying the velocity shown in figure 2 (right) by the cross-sectional area calculated from the pressure in figure 2 (left) through equation (3). The value  $R_N = 1.41 \times 10^{10} \text{ Pa s m}^{-3}$  ( $106 \text{ mmHg s ml}^{-1}$ ) is obtained.

The total compliance of each network,  $C_N$ , is determined by fitting an exponential function during the last third of diastole in the *in vivo* pressure of figure 2 (left). According to Wang *et al.* (2003), the time constant of the exponential decay is  $R_N C_N$ , which leads to  $C_N = 2.02 \times 10^{-10} \text{ m}^3 \text{ Pa}^{-1}$  ( $0.027 \text{ ml mmHg}^{-1}$ ). The total peripheral compliance is the difference between  $C_N$  and the compliance of each artery in the network, calculated

through  $A_0 l / \rho c_0^2$  (Milišić and Quarteroni 2004). The total peripheral compliance is distributed among the digital arteries in proportion to their initial cross-sectional areas.

### 3. Results and discussion

In Section 3.1 we simulate the MAT in the models of figure 1 (right) with the data shown in Appendix A, and we analyse the effect of harvesting the RA on digital outflow rates. We also study the effect of changing the location of the compression along the RA on the reversal flow peak measured by the MAT. Next, we show how a reduction in the calibre of the middle SPA (Section 3.2) and an insufficient compression of the RA (Section 3.3) affect the result of the MAT.

For each simulation we can calculate pressure and flow time histories at any site in the arterial network. We initially assume  $A(x, 0) = A_0$  and  $U(x, 0) = 0$  everywhere in the network, and we run each simulation for sufficient cardiac cycles until the waveforms become time-periodic. This typically takes around 10 cycles.

#### 3.1 Control case

Figure 4 compares the velocity in the middle point of the radial part of the SPA (SPA III) of each model before (left) and during (right) compression of the RA 15 cm proximal to the brachial bifurcation (approximately at the level of the standard pressure point in the wrist). Differences between the three anatomical variations are minimal before compression, with flow coming from the RA and moving towards the central segment of the SPA (SPA II), except for a small time interval at the end of systole. If a compression leading to total occlusion is simulated, flow becomes zero in *Model 0*, whereas flow reverses remarkably in *Models 1* and 2, because it comes from the UA through the SPA. These results are in reasonable agreement with the *in vivo* Doppler US measurements published by Zimmerman *et al.* (2001). The simulations also indicate that the reversal flow peak increases in *Models 1* and 2 as the compression point in the RA is moved away from the hand (figure 5). Hence, the peak of

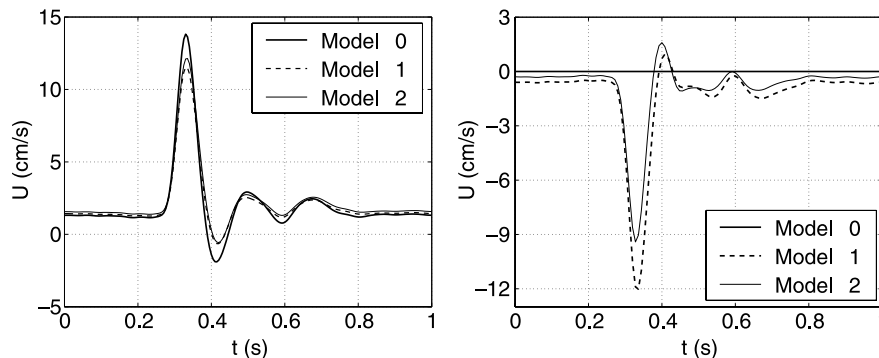


Figure 4. Velocity time histories in the middle point of the SPA III of each model before (left) and during (right) compression of the RA at the wrist.

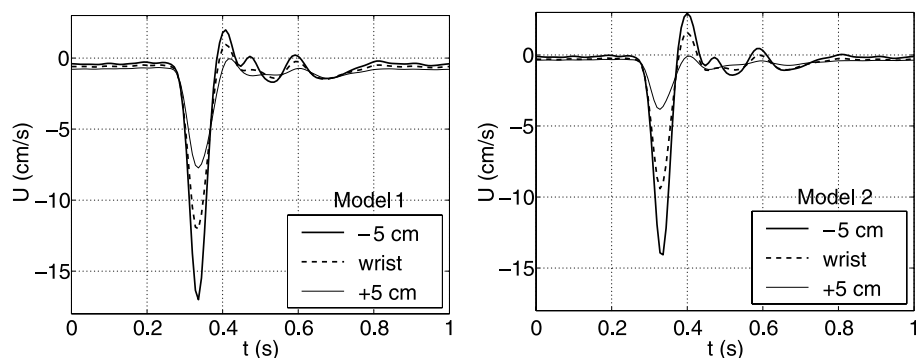


Figure 5. Effect of moving the location of compression along the RA on the flow measured in the middle point of the SPA III. Both *Models 1* (left) and 2 (right) are depicted. Compression is applied at the wrist, 5 cm distal (-5 cm) and proximal (+5 cm) to the hand.

the flow signal can be better detected by the MAT if compression is applied as far as possible from the hand.

To assess the potential risk of hand ischemia we analyse the effect of removing the RA from *Models 1* and 2 on blood supply to the fingers. Figure 6 shows flow rate over one cardiac cycle at the outlets of the digital arteries of *Models 1* (top) and 2 (bottom), when the RA is present (solid lines) and when it has been harvested (dashed lines). The results in all the digital arteries before and after harvesting do not differ significantly. Mean flow rates change less than 1% in all the digital arteries of *Model 1*, and less than 7% in all the digital arteries of *Model 2*, which suggests that changes in digital mean flow rates are small enough for the peripheral arteries to compensate for them with vasoconstriction (increase in peripheral resistance) in the digital arteries I and II and vasodilation (reduction in peripheral resistance) in the digital arteries III and IV. We also notice that the presence of the DPA in *Model 2* does not introduce significant changes in the digital flow rates predicted in *Model 1*.

Figure 6 also compares the collateral flow rates through the SPA II of *Models 1* and 2. If the RA is absent, the mean collateral flow towards the digital arteries III and IV is approximately nine times higher in *Model 1*, and seven times higher in *Model 2*. Mean flow through the DPA II of *Models 2* does not increase significantly if the RA is removed, which suggests that collateral flow takes place mainly through the SPA. Finally, we note that some ulnar collateral flow towards the digital arteries III and IV is observed in both models when the RA is present.

### 3.2 Effect of reducing the calibre of the SPA

This section studies the effect of reducing the calibre of the central SPA (SPA II) of *Models 1* and 2 on the peak of the reversal flow measured at the SPA III during occlusion of the RA, and on the mean outflows in the digital arteries III and IV after harvesting the RA. We reduce the calibre of the SPA II in the control case, referred to as 100%, in steps of 10% until it becomes zero.

Figure 7 (left) shows that *Model 1* presents a higher decrease in the peak of the reversal flow measured by

the MAT as we decrease the calibre of the SPA II than the corresponding decreases in the mean digital outflows after harvesting the RA. If the calibre of the SPA II is 30% the value of the control case, the peak reversal flow is reduced up to 80% and might be too small to be detected by Doppler US, resulting in a positive MAT. However, the mean outflow rates in the digital arteries III and IV are reduced by less than 20% when the RA is absent. Although the MAT predicts insufficient collateral flow, various compensatory mechanisms, such as vasodilatation of the digital arteries III and IV and progressive increase in the calibre of the SPA and the UA once the RA is harvested (Broadman *et al.* 2002, Zhen *et al.* 2002), are likely to increase collateral circulation to avoid hand ischemia. Therefore, the MAT is likely to produce a false-positive result. A calibre of the SPA II of 30% the value of the control case is approximately a third of the calibre of the digital artery IV. For calibres smaller than 30%, the reductions in mean digital outflows are too high and likely to lead to hand ischemia.

Figure 7 (right) shows that the DPA of *Model 2* ensures sufficient collateral flow to perfuse the digital arteries III and IV even if the SPA II is removed, in which case the mean outflow rates of the digital arteries III and IV decrease by less than 15%. However, the reversal flow peak decreases until it becomes almost zero when the calibre of the SPA II is between 50 and 40% the value of the control case, which is smaller than the calibre of the DPA II. For calibres of the SPA II smaller than 40%, the flow peak changes direction, since blood flows to the digital arteries III and IV mainly through the DPA. According to these results, the MAT clearly leads to a false-positive result for a wide range of calibres of the SPA II in *Model 2*.

If we measure the decrease in the systolic pressure of the digital arteries III and IV of *Model 1* with the compression of the RA (as proposed by Starnes *et al.* (1999)), we obtain less than 35 mmHg when the calibre of the SPA II is 30% the calibre of the control case. For calibres smaller than 25%, we obtain decreases in digital systolic pressures higher than 40 mmHg. When this test is applied to *Model 2*, the drop in digital systolic pressure is smaller than

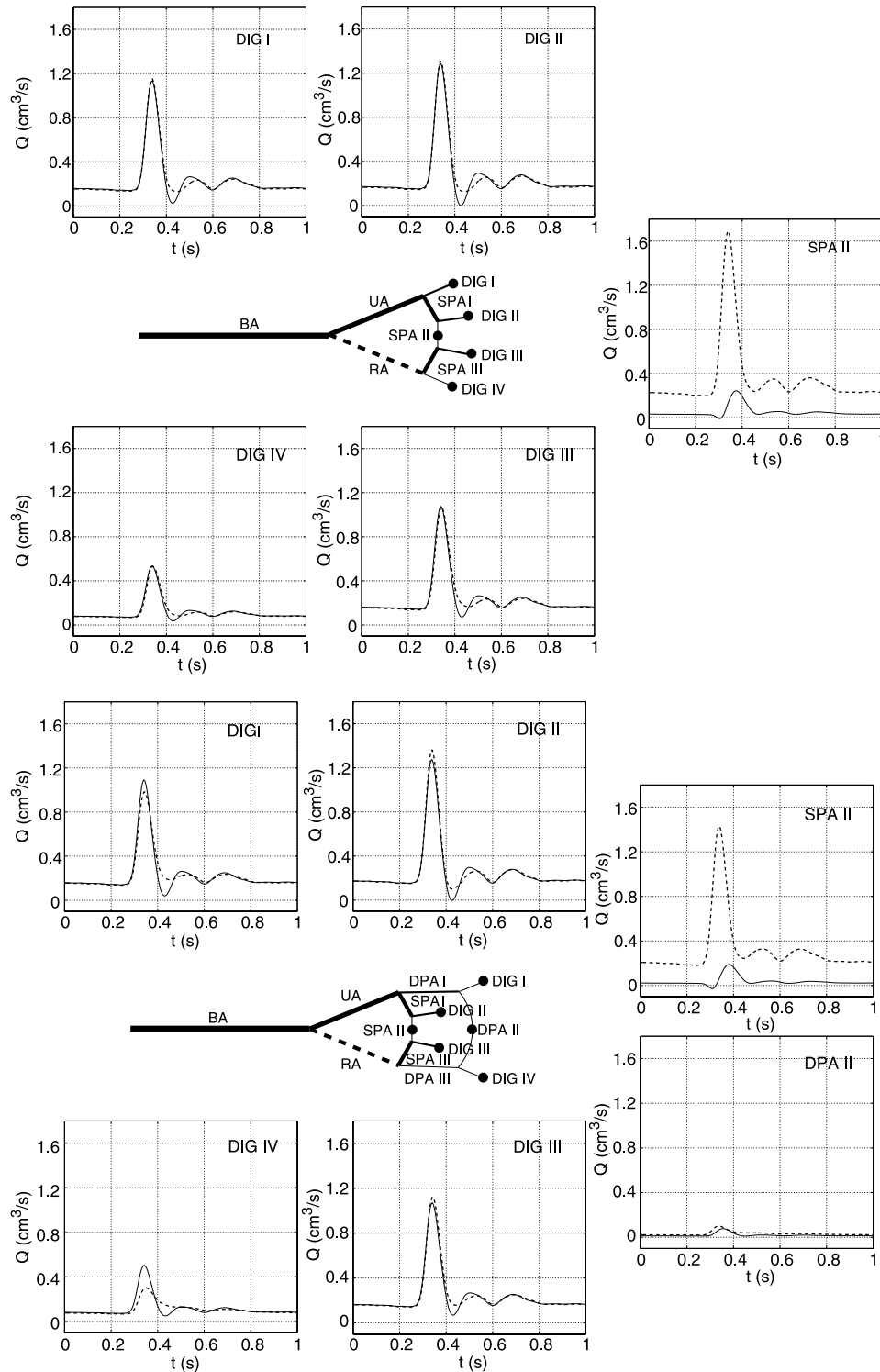


Figure 6. Flow rate time histories in the middle point of the SPA II and at the outflows of the digital arteries of *Models 1* (top) and *2* (bottom), and in the middle point of the DPA II of *Model 2*, when the RA is present (solid lines) and when it has been harvested (dashed lines). Flow rates in SPA II and DPA II are positive towards the RA.

17 mmHg in all the range of calibres of the SPA II studied. Consequently, the change in digital systolic pressure correctly detects sufficient collateral flow to perfuse the hand in all the range of calibres of the SPA II of *Models 1* and *2* studied. Zimmerman *et al.* (2001) noted that the Doppler US evidence of flow reversal in some patients may be subtle and it is prudent to consider the collateral flow

inadequate. Our 1D simulations show that the test may unnecessarily exclude some patients in these cases.

### 3.3 Effect of insufficient compression of the RA

We simulate a partial occlusion of the RA by dividing this vessel into three parts, with the centre of the middle part

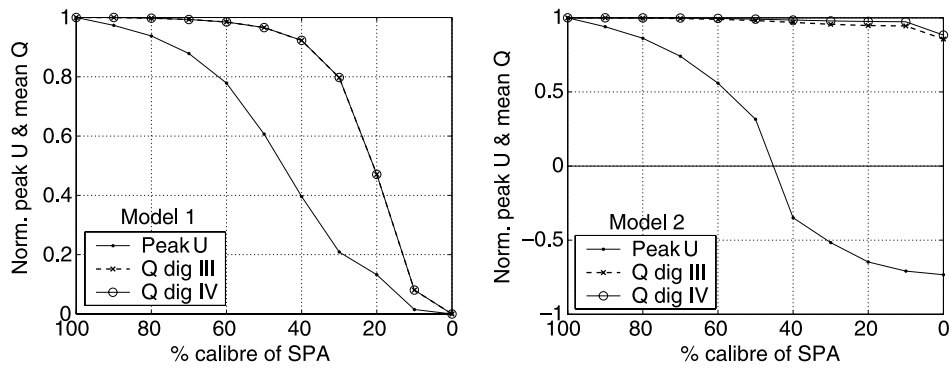


Figure 7. Effect of reducing the calibre of the SPA II of *Models 1* (left) and *2* (right) on the velocity peak in the middle point of the SPA III during occlusion of the RA at the wrist, and on the mean outflow rates in the digital arteries III and IV after harvesting the RA. Peak velocities and mean digital outflow rates are normalised by their corresponding values obtained with the calibre of the control case (100%). Negative normalised velocity peaks are directed towards the UA.

15 cm proximal to the brachial bifurcation (figure 8, top left). In the middle part, we consider  $A_0$  to be a factor  $K$  ( $0 < K < 0.2$ ) of the value in the control case.

The rest of figure 8 shows a comparison of the velocities measured in the middle point of the SPA III of the three models, when different degrees of compression of the RA are applied. A flow peak directed towards the digital artery II appears when the RA is partially occluded in *Model 0* (figure 8, top right). The value of the flow peak increases as the degree of the occlusion is reduced, since more blood flow is allowed through the RA. A partial occlusion of 90% in *Models 1* (figure 8, bottom left) and *2* (figure 8, bottom right) yields a decrease in the

corresponding reversal flow peaks of approximately half the value obtained with a total occlusion (100%), because the radial flow combines with the ulnar flow coming from the SPA. With a partial occlusion of 80%, the radial flow increases and combines with the ulnar flow to produce positive and negative flow peaks in the SPA III, which are too small to be detected by Doppler US.

According to our results, insufficient compression of the RA can lead to a false-positive MAT in arterial networks with a complete arch. The presence of a substantial flow peak in topologies without a complete arch (*Model 0*) should not lead to a false-negative MAT, since flow does not reverse.

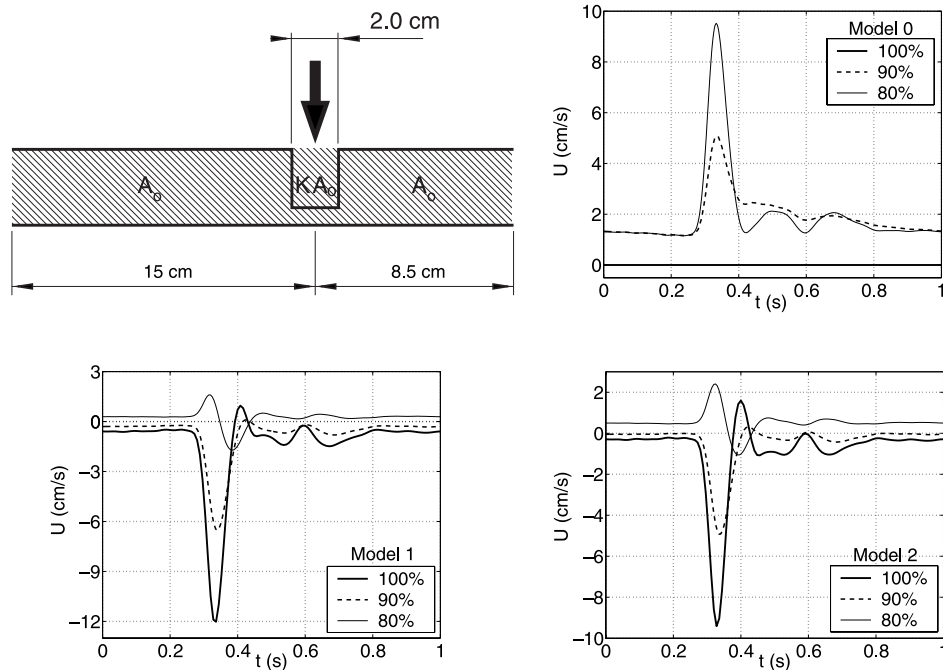


Figure 8. Simulation of a partial occlusion of the RA (top left) and velocity time histories in the middle point of the SPA III of *Model 0* (top right), *Model 1* (bottom left), and *Model 2* (bottom right) with a reduction in the cross-sectional area of the compressed part of the RA by 100, 90 and 80%. Positive velocities are directed towards the SPA II.



The change in digital systolic pressures with the compression of the RA is less than 2 mmHg for the three degrees of occlusion studied in *Models 1* and *2*, which correctly detects the presence of sufficient collateral flow. However, measurement of the variation in digital systolic pressures in *Model 0* yields a false-negative result, since a maximum drop of only 23 mmHg is obtained with a partial occlusion of 90%, and a maximum drop of 12 mmHg with a partial occlusion of 80%. These results indicate the necessity of a second Doppler probe placed over the RA to confirm complete occlusion, as suggested by Starnes *et al.* (1999).

#### 4. Conclusions

We have numerically analysed the reliability of the MAT to assess the presence of sufficient ulnar collateral blood supply to the thumb and index finger in the three most prevalent arterial anatomies in the hand. The main limitations of our simulations are the lack of detailed information on the length, cross-sectional area and elasticity of the arteries, together with more precise data on the peripheral resistances and compliances. Furthermore, all simulations have been carried out with constant peripheral resistances and, hence, the effect of autoregulation by vasoconstriction and vasodilatation has been neglected. However, these autoregulation mechanisms should not have a considerable effect on the haemodynamics of the MAT, which depends mainly on the compensatory ability of the palmar arches themselves. The effect of vasoconstriction and vasodilatation on long-term digital perfusion has already been discussed in Sections 3.1 and 3.2.

This study has shown that from a haemodynamic point of view the MAT is too cautious in selecting patients for RA graft or access for haemodialysis, since the absence of reversal flow in the radial part of the superficial palmar arch (SPA) does not always correlate to insufficient perfusion of the hand if the radial flow is interrupted. The MAT is adequate for calibres of the SPA larger than approximately a third of the calibre of the digital artery IV, and it has to be performed with a compression of the radial artery (RA) that produces an occlusion of at least 90% of the healthy initial cross-sectional area. If both conditions are satisfied, flow in the radial aspect of a complete SPA presents a large enough reversal flow peak to be detected by Doppler US (figure 4, right). The peak reversal velocity is higher and, hence, can be better detected by Doppler US, if compression at the wrist is applied as far as possible from the hand (figure 5).

This study has also proved that in anatomies with a small calibre of the central SPA, measurement of the drop in digital systolic pressures with compression of the RA can better select patients for harvesting the RA or haemodialysis access through the RA, which is in agreement with the results obtained by Starnes *et al.* (1999). However, a second Doppler probe must be placed

over the RA to confirm complete occlusion, since digital pressure measurements can fail in detecting sufficient collateral flow and, hence, lead to hand ischemia in case of insufficient radial occlusion.

#### Acknowledgements

This work was partially supported by the European Union RTN Haemodel Project (contract number HPRN-CT-2002-00270). SJS would also like to acknowledge support from an EPSRC Advanced Research Fellowship.

#### References

- J. Alastruey, "Numerical modelling of pulse wave propagation in the cardiovascular system: development, validation and clinical applications", PhD thesis, Depts. of Bioengineering and Aeronautics, Imperial College London, 2006.
- R.F. Broadman, L.E. Hirsh and R. Frame, "Effect of radial artery harvest on collateral forearm blood flow and digital perfusion", *J. Thorac. Cardiovasc. Surg.*, 123, pp. 512–516, 2002.
- R.G. Gosling, D.L. Newman, N.L.R. Bowden and K.W. Twinn, "The area ratio of normal aortic junctions", *Br. J. Radiol.*, 44, pp. 850–853, 1971.
- S.E. Greenwald and D.L. Newman, "Impulse propagation through junctions", *Med. Biol. Eng. Comput.*, 20, pp. 343–350, 1982.
- R.W. Kamienski and R.W. Barnes, "Critique of the Allen test for continuity of the palmar arch assessed by Doppler ultrasound", *Surg. Gynecol. Obstet.*, 142, pp. 861–864, 1976.
- T. Kapoor, J.L. Kaufman, J. Noshier and R.A. Sherman, *Atlas of Diseases of the Kidney*, Philadelphia: Current medicine, Inc., 1999, Vol. 5, chapter 5.
- G.E. Karniadakis and S.J. Sherwin, *Spectral/hp Element Methods for CFD*, 2nd ed. Oxford: Oxford University Press, 2003.
- H. Lippert and R. Pabst, *Arterial Variations in Man: Classification and Frequency*, Munich: J.F. Bergmann, 1985.
- F.H. Martini, *Fundamentals of Anatomy and Physiology*, 3rd ed. Englewood Cliffs, NJ: Prentice Hall, Inc., 1995.
- V. Milišić and A. Quarteroni, "Analysis of lumped parameter models for blood flow simulations and their relation with 1D models", *Math. Mod. Num. Anal.*, 38, pp. 613–632, 2004.
- S.R.A. Moraes, T.N. Araújo, A.R. Silva, A.R. Paula and J.L. Salgado, "Morphologic variations of the superficial palmar arch", *Acta Cirúrgica Brasileira*, 18, pp. 183–188, 2003.
- E. Olave, J.C. Prates, E. Mandiola, M. del Sol Calderón and C. Gabrielli, "Formaciones arteriales superficiales de la palma de la mano", *Revista Chilena de Anatomía*, 11, pp. 35–40, 1993.
- M.S. Olufsen, "Structured tree outflow condition for blood flow in larger systemic arteries", *Am. J. Physiol.*, 276, pp. H257–H268, 1999.
- G.L. Papageorgiou and N.B. Jones, "Arterial system configuration and wave reflections", *J. Biomed. Eng.*, 9, pp. 299–301, 1987.
- P. Pola, M. Serricchio, R. Flore, E. Manasse, A. Favuzzi and G.F. Posati, "Safe removal of the radial artery for myocardial revascularization: Doppler study to prevent ischemic complication to the hand", *J. Thorac. Cardiovasc. Surg.*, 112, pp. 734–737, 1996.
- J.K. Rainest, M.Y. Jaffrin and A.H. Shapiro, "A computer simulation of arterial dynamics in the human leg", *J. Biomech.*, 7, pp. 77–91, 1974.
- M. Serricchio, M. Gaudino and P. Tondi, "Hemodynamic and functional consequences of radial artery removal for coronary artery bypass grafting", *Am. J. Cardiol.*, 84, pp. 1353–1359, 1999.
- S.J. Sherwin, V. Franke, J. Peiró and K.H. Parker, "One-dimensional modelling of a vascular network in space-time variables", *J. Eng. Math.*, 47, pp. 217–250, 2003.
- N.P. Smith, A.J. Pullan and P.J. Hunter, "An anatomically based model of transient coronary blood flow in the heart", *SIAM J. Appl. Math.*, 62, pp. 990–1018, 2001.
- S.L. Starnes, S.W. Wolk, R.M. Lampman, C.J. Shanley, R.L. Prager, B.K. Kong, J.J. Fowler, J.M. Page, S.L. Babcock, L.A. Lange, E.E. Erlandson and W.M. Whitehouse, Jr, "Noninvasive evaluation of hand

- circulation before radial artery harvest for coronary artery bypass grafting", *J. Thorac. Cardiovasc. Surg.*, 117, pp. 261–266, 1999.
- N. Stergiopoulos, D.F. Young and T.R. Rogge, "Computer simulation of arterial flow with applications to arterial and aortic stenoses", *J. Biomech.*, 25, pp. 1477–1488, 1992.
- J.J. Wang, A.B. O'Brien, N.G. Shrive, K.H. Parker and J.V. Tyberg, "Time-domain representation of ventricular-arterial coupling as a windkessel and wave system", *Am. J. Heart Circ. Physiol.*, 284, pp. H1358–H1368, 2003.
- J.T. Winterer, J. Ennker, K. Scheffler, U. Rosendahl, O. Schafer, M. Wanner, J. Laubenberger and M. Langer, "Gadolinium-enhanced elliptically reordered three-dimensional MR angiography in the assessment of hand vascularization before radial artery harvest for coronary artery bypass grafting: first experience", *Investigat. Radiol.*, 36, pp. 501–508, 2001.
- W. Zhen, H. Tong, Y. Wang, Y. Sun, W. Huan, Y. Ma, J. Tian and L. Wu, "Coronary bypass revascularization with radial artery and internal mammary artery grafts", *Chin. Med. J.*, 115, pp. 55–57, 2002.
- P. Zimmerman, E. Chin, S. Laifer-Narin, N. Ragavendra and E.G. Grant, "Radial artery mapping for coronary artery bypass graft placement", *Radiology*, 220, pp. 299–302, 2001.

## Appendix A: Physiological data of each model

Table A1. Physiological data used in *Model 0*.

Arterial segment	Length (cm)	$R_0$ (cm)	Wave speed ( $\text{m s}^{-1}$ )	Peripheral resistance ( $10^{10} \text{ Pa s m}^{-3}$ )	Peripheral compliance ( $10^{-11} \text{ m}^3 \text{ Pa}^{-1}$ )
Brachial	42.2	0.249	9.2	–	–
Ulnar	23.8	0.203	10.4	–	–
Radial	23.5	0.174	10.8	–	–
Digital I	2.5	0.130	12.1	5.13	1.63
Digital II	3.0	0.136	11.1	4.69	1.79
Digital III	3.0	0.132	13.8	5.01	1.67
Digital IV	1.5	0.093	13.6	10.00	0.84
SPA I	1.0	0.169	11.1	–	–
SPA III	1.0	0.161	12.1	–	–

Table A2. Physiological data used in *Model 1*.

Arterial segment	Length (cm)	$R_0$ (cm)	Wave speed ( $\text{m s}^{-1}$ )	Peripheral resistance ( $10^{10} \text{ Pa s m}^{-3}$ )	Peripheral compliance ( $10^{-11} \text{ m}^3 \text{ Pa}^{-1}$ )
Brachial	42.2	0.249	9.2	–	–
Ulnar	23.8	0.203	10.4	–	–
Radial	23.5	0.174	10.8	–	–
Digital I	2.5	0.130	12.1	5.13	1.63
Digital II	3.0	0.136	11.1	4.69	1.79
Digital III	3.0	0.132	13.8	5.01	1.67
Digital IV	1.5	0.093	13.6	10.00	0.84
SPA I	1.0	0.169	11.1	–	–
SPA II	1.0	0.114	14.5	–	–
SPA III	1.0	0.161	12.1	–	–

Table A3. Physiological data used in *Model 2*.

Arterial segment	Length (cm)	$R_0$ (cm)	Wave speed ( $\text{m s}^{-1}$ )	Peripheral resistance ( $10^{10} \text{ Pa s m}^{-3}$ )	Peripheral compliance ( $10^{-11} \text{ m}^3 \text{ Pa}^{-1}$ )
Brachial	42.2	0.249	9.2	–	–
Ulnar	23.8	0.203	10.4	–	–
Radial	23.5	0.174	10.8	–	–
Digital I	2.5	0.130	12.1	5.13	1.59
Digital II	3.0	0.136	11.1	4.69	1.74
Digital III	3.0	0.132	13.8	5.01	1.63
Digital IV	1.5	0.093	13.6	10.00	0.81
SPA I	1.0	0.169	11.1	–	–
SPA II	1.0	0.114	14.5	–	–
SPA III	1.0	0.161	12.1	–	–
DPA I	3.0	0.130	12.1	–	–
DPA II	3.0	0.075	14.5	–	–
DPA III	3.0	0.093	13.6	–	–